

# Nonideal evolution of nonaxisymmetric, force-free magnetic fields in a magnetar

A. Mastrano<sup>1\*</sup> and A. Melatos<sup>1†</sup>

<sup>1</sup>*School of Physics, University of Melbourne, Parkville VIC 3010, Australia*

Accepted ?. Received ?; in original form ?

## ABSTRACT

Recent numerical magnetohydrodynamic calculations by Braithwaite and collaborators support the ‘fossil field’ hypothesis regarding the origin of magnetic fields in compact stars and suggest that the resistive evolution of the fossil field can explain the reorganisation and decay of magnetar magnetic fields. Here, these findings are modelled analytically by allowing the stellar magnetic field to relax through a quasistatic sequence of nonaxisymmetric, force-free states, by analogy with spheromak relaxation experiments, starting from a random field. Under the hypothesis that the force-free modes approach energy equipartition in the absence of resistivity, the output of the numerical calculations is semiquantitatively recovered: the field settles down to a linked poloidal-toroidal configuration, which inflates and becomes more toroidal as time passes. A qualitatively similar (but not identical) end state is reached if the magnetic field evolves by exchanging helicity between small and large scales according to an  $\alpha$ -dynamo-like, mean-field mechanism, arising from the fluctuating electromotive force produced by the initial random field. The impossibility of matching a force-free internal field to a potential exterior field is discussed in the magnetar context.

**Key words:** MHD – plasmas – stars: magnetic fields – stars: neutron

## 1 INTRODUCTION

Magnetars are neutron stars whose (un)pulsed X-ray luminosities ( $\lesssim 10^{29}$  W) exceed their spin-down luminosities (Thompson & Duncan 1995). They fall into two classes: soft gamma repeaters (SGRs) (Rothschild et al. 1994; Hurley et al. 2005) and anomalous X-ray pulsars (AXPs) (Thompson & Duncan 1996; Mereghetti 2000; McLaughlin et al. 2003; Woods & Thompson 2006). From their observed spin periods and spin-down rates, one can infer that magnetars possess very high surface magnetic fields  $B \geq 5 \times 10^9$  T<sup>1</sup>, higher than most (although not all) rotation-powered pulsars (Kouveliotou et al. 1998; Melatos 1999; Kaspi & McLaughlin 2005). Duncan and Thompson (1992) proposed that the resistive decay of the magnetic field powers the continuous X-ray emission from AXPs and the intense outbursts (lasting a fraction of a second) from SGRs, e.g. Palmer et al. (2005). AXPs may be SGRs which are yet to burst (Thompson & Duncan 1996; Mereghetti 2000).

It remains unclear how such strong stellar magnetic fields come to exist. Broadly speaking, there are two hypotheses for their origin (Braithwaite & Spruit 2006): (1) fossil field, where the progenitor star’s magnetic field is amplified by compression during core collapse and is frozen into the highly conducting compact remnant; and (2) dynamo amplification, where the field is generated by a convective dynamo in the proto-neutron star. (In this paper, we discuss dynamos operating in the protostar stage rather than continuously regenerating the magnetic field of a neutron star, white dwarf, or Ap star during the star’s lifetime; the latter idea seems to be ruled out by observations of Ap stars and white dwarfs, as we discuss below.) Observations to date do not favour conclusively one hypothesis over the other. Indeed, the hypotheses are not mutually exclusive; a dynamo operating in the protoneutron star/white dwarf stage may amplify the fossil field inherited from the main sequence. Fossil fields are supported by

\* E-mail: amastran@physics.unimelb.edu.au

† E-mail: amelatos@physics.unimelb.edu.au

<sup>1</sup> Throughout this paper, we use SI units. 1 T =  $10^4$  G.

the observed magnetic field distribution in Ap stars and white dwarfs (Ferrario & Wickramasinghe 2006). On the other hand, the magnetar birth rate implied by observations agrees with the operation of a large-scale dynamo in rapidly rotating, massive proto-neutron stars (with masses  $\gtrsim 25M_{\odot}$  and periods  $\sim 1$  ms) (Kouveliotou et al. 1994; Gaensler, Gotthelf, & Vasisht 1999; Heger et al. 2003; Gaensler et al. 2005; Popov & Prokhorov 2006). On the theoretical front, one of the major issues with the fossil field hypothesis is the (in)stability of the progenitor field. Much work has been done to show that purely poloidal and purely toroidal field configurations are unstable (Prendergast 1956; Wright 1973; Goossens & Tayler 1980; van Assche, Tayler, & Goossens 1982), but a linked toroidal-poloidal configuration may be stable (Tayler 1980).

There are, in fact, two different fossil field hypotheses: “strong”, where the magnetic field of the progenitor is  $\sim 1$  T for a  $1M_{\odot}$  star, following compression of a strongly magnetised ( $3 \times 10^{-2}$  T) molecular cloud (Moss 2001, 2003), and “weak”, where the field is generated after the progenitor forms by various dynamo processes [see e.g., Charbonneau & MacGregor (1996) and Spruit (2002)]. In this paper, we do not distinguish between the two hypotheses, as our analysis is too elementary to treat the magnetization of the progenitor. Magnetic flux conservation implies that a magnetar progenitor needs to have magnetic field strength  $B \gtrsim 1$  T (Woltjer 1964; Vink & Kuiper 2006). The core and envelope of the progenitor are strongly coupled, angular momentum is rapidly transferred away by a stellar wind, and the core rotates rather slowly, for example  $P \sim 10$  ms for  $15 M_{\odot}$  stars and  $P \sim 4$  ms for  $35 M_{\odot}$  stars (Spruit 2002; Heger, Woosley, & Spruit 2005). This is slower than the  $P \sim 1$ – $3$  ms needed for an efficient dynamo to operate (Duncan & Thompson 1992; Thompson & Duncan 1995, 1996; Heger et al. 2005; Vink 2008). Heger et al. (2005) calculated the effects of magnetic braking on newly born neutron stars and concluded that  $P \lesssim 3$  ms is achieved only in stars with  $M \gtrsim 25M_{\odot}$  (Gaensler et al. 2005; Heger et al. 2005). The requirement of rapid rotation suggests a stringent absolute test of the dynamo hypothesis: are enough neutron stars born with such rapid rotations to explain the observed magnetar birth rate? Taking  $25M_{\odot}$  to be the mass cutoff, Gaensler *et al.* (2005) estimated the birth rate of magnetars to be  $\sim 10\%$  that of radio pulsars, consistent with current populations of AXPs and SGRs (Kouveliotou et al. 1994; Gaensler et al. 1999). In contrast, the explosion energies of the supernova remnants associated with the AXPs 1E 1841–045 (Kes 73) and 1E2259+586 (CTB109) and the SGR 0526–66 (estimated from the shock speed, which is determined from X-ray spectra measured by *XMM-Newton*) suggest an initial spin period  $P \gtrsim 5$  ms, not enough for a dynamo (Vink & Kuiper 2006; Vink 2008).

The lack of correlation between the observed field strength and spin periods of Ap stars and white dwarfs seems to argue against the hypothesis that a dynamo can operate in the core to regenerate the magnetic field continuously (Braithwaite & Spruit 2004; Petit et al. 2007). Observations of main sequence stars that are potential magnetar progenitors do not conclusively favour either fossil fields or protostar dynamos. From the similar fluxes of magnetic A stars (called Ap stars) and white dwarfs, Ferrario and Wickramasinghe (2006) inferred that O and B progenitors need to have dipolar fields of strength  $10^{-4}$  T  $\lesssim B \lesssim 10^{-1}$  T to generate neutron stars with  $10^7$  T  $\lesssim B \lesssim 10^{11}$  T. Unfortunately, the magnetic fields of these O and B stars are hard to observe. This is because their absorption lines in the optical range are few and broad (perhaps due to rotation), making the Zeeman effect, by which the magnetic fields are measured, harder to detect (Donati et al. 2006a, b; Vink 2008). Two magnetic stars, HD 191612 (O class) and  $\tau$  Sco (B class), are observed to have fairly long periods, 41 and 538 days respectively, which are inconsistent with the dynamo hypothesis (Donati et al. 2006a, b). Note, however, that their current rotation periods may not reflect directly on their periods during the protostar phase [many processes, such as accretion disk locking, can slow down the star after the stable field is in place (Braithwaite 2008)]. So, while the magnetic field today may not be generated continuously by a dynamo, it may arise from a dynamo during the protostar stage. It must also be kept in mind that our knowledge of magnetism in main sequence stars of masses  $> 8M_{\odot}$  is sketchy.

Recent magnetohydrodynamic (MHD) simulations have shown that an unstable, random initial field can decay into a long-term stable configuration (Braithwaite & Nordlund 2006; Braithwaite & Spruit 2004, 2006). Starting from a random magnetic field, the simulations follow the field as it relaxes towards a lower energy state, with and without diffusion, transforming spontaneously into a stable configuration: a nearly axisymmetric torus with roughly equal poloidal and toroidal fluxes, which expands as a function of time. Poloidal field lines are wrapped around the torus, extending through the atmosphere and creating an ‘approximate dipole’ (Braithwaite & Nordlund 2006). It must be noted that the results of the cited numerical simulations do not say anything directly about whether a neutron star’s field comes from a dynamo process operating during the protoneutron star phase or simply conserved from the main sequence progenitor. A stable magnetic field configuration is necessary in both fossil field and dynamo hypotheses.

Motivated by these numerical simulations, we ask here whether it is possible to model the magnetic evolution approximately yet analytically as a slow, helicity-conserving relaxation through a quasistatic sequence of force-free states, by analogy with spheromak experiments. A previous paper on relaxing force-free magnetic fields focused on axisymmetric modes (Broderick & Narayan 2007). In this work, we draw particular attention to the importance of nonaxisymmetric modes, without which it is impossible to reproduce the linked poloidal-toroidal field lines observed in the simulations (Braithwaite & Nordlund 2006; Braithwaite & Spruit 2004, 2006). We also allow our model neutron star to develop a small-scale turbulent velocity field as the magnetic field relaxes, generalizing Broderick and Narayan’s (2007) work to accommodate (some of) the physics of a mean-field dynamo (Blackman & Field 2004).

In Section 2, we delineate our aim and the four hypotheses regarding the nondiffusive evolution of the force-free field

that we investigate. In Section 3, we discuss the basic properties of force-free magnetic fields in detail. Then, in Section 4, we discuss the results of our study of the nondiffusive evolution of a composite force-free field through the four different hypotheses. In Section 5, we briefly discuss the diffusive evolution of a force-free field. Finally, in Section 6, we present our conclusions and discuss in greater detail the fundamental problem of matching a force-free magnetic field to a potential field.

## 2 EVOLUTIONARY HYPOTHESES

The aim of this paper is to construct a simple, *approximate*, analytic model for the evolution of magnetar fields (via non-diffusive and diffusive processes), which reproduces coarsely the numerical results of Braithwaite and collaborators. In pursuing this objective, we hypothesize that the field evolves according to two principles: (1) it passes quasistatically through a series of force-free equilibria, each a superposition of axisymmetric and nonaxisymmetric modes; and (2) the relative weightings of the modes are controlled by the conservation (or slow evolution) of global quantities like magnetic helicity, energy, or hydrodynamic vorticity. Obviously, this approach sacrifices realism for simplicity; it is emphatically not a substitute for high-resolution, resistive MHD simulations.

We choose force-free fields as our basis because of their astrophysical prevalence (Priest 1984) and analytic simplicity. This choice is justified by laboratory experiments with spheromaks, which are topologically congruent with a star, where it is observed that a spherical magnetic field relaxes into a force-free axisymmetric state, known as the Taylor state (Rosenbluth & Bussac 1979; Goldenbaum et al. 1980; Yamada et al. 1981; Janos et al. 1985; Taylor 1986). In a magnetar, the force-free approximation is defensible with respect to latitudinal and azimuthal force components, with  $\nabla p \ll \mu_0^{-1}(\nabla \times \mathbf{B}) \times \mathbf{B}$  in these directions (where  $p$  is the pressure and  $\mathbf{B}$  is the magnetic field). The approximation breaks down in the radial direction in a realistic star, due to the strong gravitational force. However, the main aim of this paper is to make contact with the MHD simulations of Braithwaite and collaborators. For this purpose, as noted below, the force-free approximation is adequate overall.

We stress here that nothing physical requires the field to be force-free; indeed, with  $\nabla p \gg \mathbf{J} \times \mathbf{B}$ , one would naïvely expect  $\mathbf{B}$  to be anything but force-free (at least with regard to the radial gradients). We want to make it clear that we do not propose force-free fields as a realistic model, but rather as a convenient mathematical artifice for studying the long-term evolution of magnetic helicity and field geometries in a neutron star. That is, we take the simplifying assumption that the field is force-free, to see whether the behaviour of such a field mimics that of a more general field investigated by Braithwaite et al. Additionally:

(i) Force-free fields are an analytically convenient orthonormal basis in which any interior field can be expanded. It will be worth testing empirically (from the simulation output) what the coefficients in a force-free expansion are, in view of the qualitative visual agreement with the simulation results reported in Sections 4 and 5.

(ii) In many other high- $\beta$  ( $|\nabla p| \gg |\mathbf{J} \times \mathbf{B}|$ ) plasmas, e.g., in spheromaks (Jarboe et al. 1980; Turner et al. 1983; Janos et al. 1985; Barnes et al. 1986; Knox et al. 1986), the field does relax to a force-free (minimum energy) state (Taylor 1986), even though it does not have to and one naïvely would not expect it to. It does this by tending “thermodynamically” to a state with  $\nabla p \approx 0$  and  $\mathbf{J} \times \mathbf{B} \approx 0$  separately (because a magnetic field does no work in the first law of thermodynamics). The analogue here is a state with  $-\nabla p + \rho \nabla \Phi \approx 0$  and  $\mathbf{J} \times \mathbf{B} \approx 0$ .

The MHD simulations cited above start from a random field. The random field is not force free, but this is immaterial: the role played by the initial state, in our model, is to define the initial values of conserved (or nearly conserved) global quantities like magnetic helicity. We focus on the three lowest poloidal orders of the magnetic field, including nonaxisymmetric modes. Our initial state is a sum of these modes, equally weighted to emulate a random field (i.e., spatially uncorrelated) where all modes (up to some wavenumber cutoff) are equally probable.

Next, we entertain four possibilities for how the field evolves *without diffusion*, as in the first stage of the numerical simulations of Braithwaite and Nordlund (2006). One possible end state of nondiffusive evolution is energy equipartition, where each force-free mode contributes equal energy to the total, Sec. 4.2 explains the equipartition assumption in more detail. We conjecture that a random field may evolve into an equipartitioned state either by keeping the total energy and helicity constant (state A) or by keeping the total helicity constant while allowing the energy to vary (state B). A second possible end state of nondiffusive evolution is dictated by the dynamo theory of Blackman and Field (2004), in which helicity is exchanged between short- and long-wavelength modes through the agency of a turbulent electromotive force ( $\alpha$  effect). Again, the end state is reached either by keeping the total energy and helicity constant (state C) or by keeping the total helicity constant while allowing the energy to vary (state D). The discretisation scheme of the simulation gives rise to a small “effective diffusivity”, which leads to some dissipation and energy loss (by a factor of  $\sim 10 - 100$ ) during the initial relaxation, before a stable magnetic field configuration forms (Braithwaite 2008). In our analysis, however, we prefer to keep an open mind and allow cases without (A and C) and with (B and D) energy loss.

Lastly, we briefly discuss how the relaxed, force-free field diffuses over long times when the electrical resistivity is not

zero. In the numerical simulations, the magnetic field is observed to diffuse out of the star in a roughly dipolar configuration (Braithwaite & Nordlund 2006). We show that a field which is a linear combination of several force-free modes diffuses while keeping the force-free parameter  $a$  (defined in Section 3) and relative weighting of the modes constant, thus retaining its pre-diffusion shape. We also discuss the difficulty of matching a force-free field with spatially uniform  $a$  to a potential field outside the star.

### 3 NONAXISYMMETRIC FORCE-FREE FIELDS

Force-free magnetic fields obey the condition  $\nabla \times \mathbf{B} = a\mathbf{B}$ , where  $a(\mathbf{x})$  (units: inverse length) is a function of position in general. The conduction current density,  $\mathbf{J} = \mu_0^{-1} \nabla \times \mathbf{B}$ , is therefore parallel to  $\mathbf{B}$  and the Lorentz force, proportional to  $\mathbf{J} \times \mathbf{B}$ , vanishes. Hence, force-free fields offer an attractive, static, *long-term* magnetic configuration. In general, the solution to the force-free condition that also fulfills  $\nabla \cdot \mathbf{B} = 0$  can be written as (Chandrasekhar & Kendall 1957; Priest 1984)

$$\mathbf{B} = a\nabla \times (\psi \mathbf{n}) + \nabla \times [\nabla \times (\psi \mathbf{n})] \quad (1)$$

where  $\mathbf{n}$  is some vector and  $\psi$  is a scalar solution of the Helmholtz equation

$$(\nabla^2 + a^2)\psi = 0. \quad (2)$$

In spherical polar coordinates  $(r, \theta, \phi)$ , choosing  $\mathbf{n} = \hat{\mathbf{e}}_r$  and restricting attention (for simplicity) to uniform  $a$ , we can write the magnetic field as (Priest 1984)

$$B_r = \sum_{n=1}^{\infty} \sum_{m=0}^n C_{nm} n(n+1) r^{-3/2} J_{n+1/2}(ar) P_n^m(\cos \theta) \exp(im\phi), \quad (3)$$

$$B_\theta = \sum_{n=1}^{\infty} \sum_{m=0}^n C_{nm} [ar^{-1/2} J_{n-1/2}(ar) - nr^{-3/2} J_{n+1/2}(ar)] \frac{dP_n^m(\cos \theta)}{d\theta} \exp(im\phi) \\ + C_{nm} imar^{-1/2} J_{n+1/2}(ar) P_n^m(\cos \theta) \exp(im\phi) / \sin \theta, \quad (4)$$

$$B_\phi = \sum_{n=1}^{\infty} \sum_{m=0}^n C_{nm} im [nr^{-3/2} J_{n+1/2}(ar) - ar^{-1/2} J_{n-1/2}(ar)] P_n^m(\cos \theta) \exp(im\phi) / \sin \theta \\ - C_{nm} ar^{-1/2} J_{n+1/2}(ar) \frac{dP_n^m(\cos \theta)}{d\theta} \exp(im\phi), \quad (5)$$

where  $C_{nm}$  are complex constants,  $J_{n\pm 1/2}$  denotes Bessel functions of order  $n \pm 1/2$ , and  $P_n^m$  denotes associated Legendre functions of the first kind. Physical field components are the real parts of (3)–(5). We plot some of these modes in Fig. 1. The leftmost plot in the top row shows the axisymmetric Taylor state, the end state achieved by relaxing spheromak magnetic fields (Taylor 1986). Note that a nonaxisymmetric vector field may have chaotic (albeit closed) field lines (e.g. second row, centre plot, Fig. 1) even though the vector field is smooth, because the field line equations form a nonlinear dynamical system of dimension three (Botha & Evangelidis 2004). The field lines are closed (because  $\nabla \cdot \mathbf{B} = 0$ ) but chaotic (two field lines that are arbitrarily close at some point will diverge macroscopically along their length). By contrast, the field lines of an axisymmetric vector field must form simple loops, by the Poincaré-Bendixson theorem for two-dimensional dynamical systems (Jordan & Smith 1999).

A nonuniform  $a$  gives an extra term in the diffusion equation, since  $\eta \nabla^2 \mathbf{B} = -a^2 \eta \mathbf{B} - \eta (\nabla a) \times \mathbf{B}$ . Under the action of the new term, the field changes shape as it diffuses. In addition, a nonuniform  $a$  facilitates global current closure, since the currents carried by two flux tubes of equal area (proportional to the local value of  $a$ ) are not necessarily equal if  $a$  varies from place to place. This allows return currents to be confined to thin sheets that leave most of the field undisturbed, helping greatly with the matching problem discussed in Sec. 6.

#### 3.1 Helicity

The magnetic helicity within a volume  $V$  is defined as

$$H = \int_V dV \mathbf{A} \cdot \mathbf{B}, \quad (6)$$

where  $\mathbf{A}$  is the vector potential. It has been argued theoretically (Taylor 1986), and observed in spheromak experiments (Jarboe et al. 1980; Turner et al. 1983; Janos et al. 1985; Barnes et al. 1986; Knox et al. 1986), that  $H$  remains constant as a force-free field relaxes. More generally, if a nonzero electric field  $\mathbf{E} = -\nabla \phi - \partial \mathbf{A} / \partial t$  is included (where  $\phi$  is the scalar

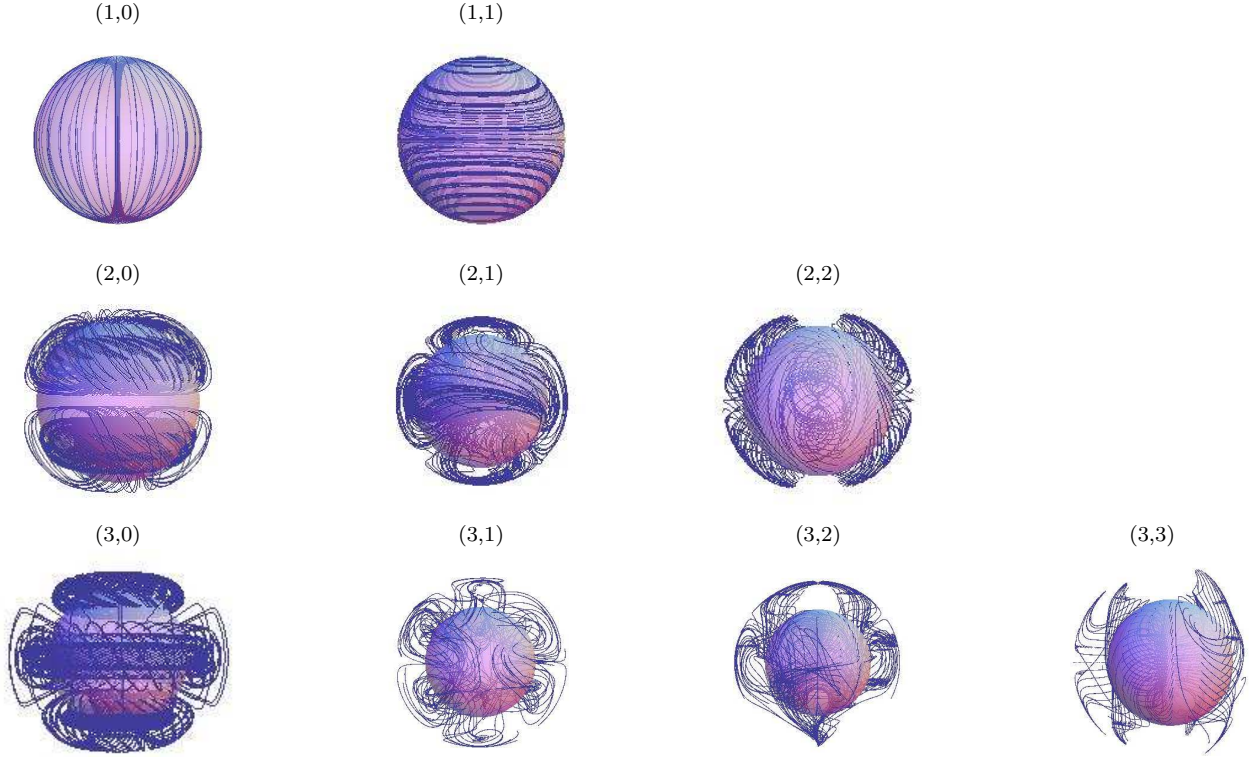


**Figure 1.** Magnetic field lines for the force-free modes  $1 \leq n \leq 3$ ,  $0 \leq m \leq n$ , with the magnetic foot points (the starting points for the field line integration) initialised at  $ar_s = 4.49$ ,  $\arccos(\theta) = (-8/9, -7/9, \dots, 7/9, 8/9)$ ,  $\phi = (0, \pi/8, \pi/4, \dots, 15\pi/8)$ . Each panel is labelled by  $(n, m)$ . The north-south axis lies vertical in the plane of the page.

potential), Faraday's law and the definitions of  $H$  and  $\mathbf{A}$  imply  $dH/dt = d(\mathbf{A} \cdot \mathbf{B})/dt = -2\mathbf{E} \cdot \mathbf{B} + \nabla \cdot (\phi\mathbf{B} + \mathbf{A} \times \mathbf{E})$ , which one can then integrate over a volume  $V$  to obtain (Brandenburg & Subramanian 2005)

$$\frac{dH}{dt} = -2 \int_V dV \mathbf{E} \cdot \mathbf{B} + \int_{\partial V} d\mathbf{S} \cdot (\mathbf{A} \times \mathbf{E} + \phi\mathbf{B}). \quad (7)$$

The helicity is gauge-independent if  $\mathbf{B}$  is strictly tangential on the bounding surface  $\partial V$ , which is true for spheromaks but not for a neutron star, unless we extend  $\partial V$  to infinity. This makes sense only if  $\mathbf{B}$  falls off fast enough, such that  $H$  is finite. To achieve this, the force-free field [which scales as  $|\mathbf{B}| \propto r^{-1}$  for large  $r$ , according to (3)–(5)] must be matched to a potential field at  $r = r_s$  (where  $r_s$  is the surface of the star), something that is difficult to do both in practice and in principle (Sec. 6 further explains why) (Wheatland 2006). Consequently, in this paper, we assume that the field is force-free everywhere while integrating over the volume  $r \leq r_s$  in (6) to keep  $H$  finite. The results in Sections 4–5 must be interpreted with this approximation in mind.

The reader should note that, for simplicity's sake, we implicitly assume that the field at  $r > r_s$  is also described by Eqs. (3)–(5), not by a potential field. This means that, at infinity, the magnetic field does not approach a dipole field (which is physically unrealistic and contrary to pulsar observations). Ideally, we wish to use an external field which is more realistic, such as a dipole field or a dipole-dominated multipole field, but this raises the issue of boundary matching, which is nontrivial and is discussed further in Sec. 6.

### 3.2 Energy

In a force-free field with uniform  $a$ , we have  $H = \int_V dV \mathbf{A} \cdot \mathbf{B} = (1/a) \int_V dV \mathbf{B}^2 = 2\mu_0 W/a$ , where  $W$  is the total magnetic energy and  $\mu_0$  is the magnetic permeability of free space. This is true both for each mode  $(n, m)$  in (3)–(5) and for a linear superposition of modes; it can be easily verified by direct integration that the cross-terms  $\int_V dV \mathbf{B}_{(l_1, m_1)} \cdot \mathbf{B}_{(l_2, m_2)}$  with  $l_1 \neq l_2$  and/or  $m_1 \neq m_2$  all vanish because of the linear independence of the modes. For a particular value of  $a$ , higher mode numbers have higher energies. Fig. 2 illustrates this trend for modes with  $1 \leq n \leq 3$  by graphing  $W$  against  $a$  for fixed  $r_s$ . The modes  $(n, m) = (1, 0)$  and  $(1, 1)$  have equal energies, despite having different structures, because the energies in their radial and tangential components are separately equal.

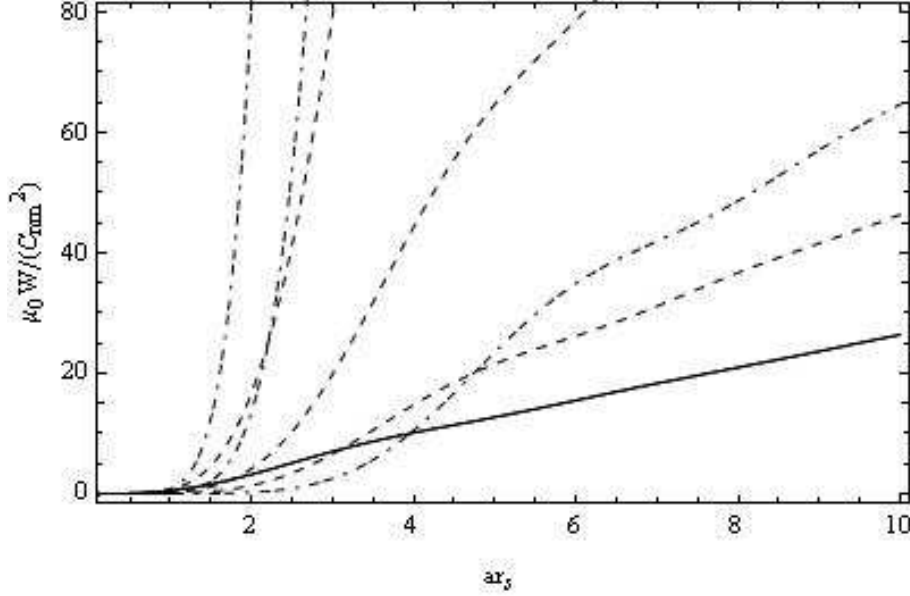


**Figure 2.** Magnetic energy  $W_{nm}$  for the force-free mode  $(n, m)$  in (3)–(5) (in units of  $C_{nm}^2/\mu_0$  as a function of  $ar_s$ , where  $a$  is the force-free parameter and  $r_s$  is the radius of the star. Solid curves:  $n = 1$ ; dashed curves:  $n = 2$ ; dashed-dotted curves:  $n = 3$ . For each value of  $n$ , the lowest curve corresponds to the axisymmetric ( $m = 0$ ) and the highest curve corresponds to the  $m = n$  mode. Note that  $W_{10} = W_{11}$  and  $W_{30} = W_{31}$ .

Taking the dot product of Faraday’s law with  $\mathbf{B}/(2\mu_0)$ , then using  $\mathbf{E} = \mathbf{J}/\sigma - \mathbf{v} \times \mathbf{B}$  to eliminate  $\mathbf{E}$ , and finally integrating over a volume  $V$ , one obtains the following equation for energy evolution (Brandenburg & Subramanian 2005),

$$\frac{dW}{dt} = - \int_V dV (\mathbf{J} \times \mathbf{B}) \cdot \mathbf{v} - \frac{1}{\sigma} \int_V dV \mathbf{J}^2 - \frac{1}{\mu_0} \int_{\partial V} d\mathbf{S} \cdot \mathbf{E} \times \mathbf{B}, \quad (8)$$

where  $\mathbf{v}$  is the velocity of the charged fluid threaded by  $\mathbf{B}$ ,  $\sigma$  is the conductivity, and  $\mathbf{J}$  is the current density. For force-free fields, one can write  $\mu_0 \mathbf{J} = \nabla \times \mathbf{B} = a\mathbf{B}$ . Thus, the first term on the right-hand side of Eq. (8) vanishes, giving  $\mathbf{E} \times \mathbf{B} = (\mathbf{J}/\sigma - \mathbf{v} \times \mathbf{B}) \times \mathbf{B} = -(\mathbf{v} \times \mathbf{B}) \times \mathbf{B}$  and hence

$$\frac{dW}{dt} = - \frac{a^2}{\mu_0^2 \sigma} \int_V \mathbf{B}^2 dV + \frac{1}{\mu_0} \int_V d\mathbf{S} \cdot [(\mathbf{v} \times \mathbf{B}) \times \mathbf{B}]. \quad (9)$$

## 4 PRE-DIFFUSION EVOLUTION

The numerical experiments of Braithwaite and collaborators (Braithwaite & Nordlund 2006; Braithwaite & Spruit 2004, 2006) proceeded in two stages. In the first stage, a random magnetic field threading a stationary ball of plasma is loaded into a three-dimensional MHD solver with both numerical and physical resistivities. We study the ideal-MHD evolution in this section. In the second stage, the collisional resistivity is switched on. We study the resistive evolution in Section 5. Note that we do not mean to imply here that the only diffusion process is Spitzer resistivity [another possibility is, for example, ambipolar diffusion (Goldreich & Reisenegger 1992)]. Our results apply regardless of the actual diffusion mechanism, provided it is isotropic (i.e.,  $\sigma$  is a scalar).

### 4.1 Initial conditions: random field

Braithwaite and Nordlund (2006) initialised their simulation with a random field, whose maximum wavenumber in a Fourier decomposition is set by the grid scale ( $\sim 10^2 R_*^{-1}$ ). We simulate the initial state as a linear combination of the modes  $1 \leq n \leq 3$ ,  $0 \leq m \leq n$ , in which the modes are equally weighted, i.e. all constants  $C_{nm}$  are set to be equal. We draw the field lines of the initial state in Fig. 4a. Note that the maximum wavenumber is  $k_{\max} \approx 4.2\pi$  (for  $n = m = 3$ ). One can readily increase  $k_{\max}$  by increasing  $n$  to match Braithwaite and Nordlund’s (2006) experiment, but there is no need; the conserved global quantities are approximated to  $\sim 10\%$  with  $n \leq 3$ .

Note that the total energy  $W_T = \sum_{n=1}^3 \sum_{m=0}^n W_{nm}$  for our initial state is minimised at  $a = 7.0$ .

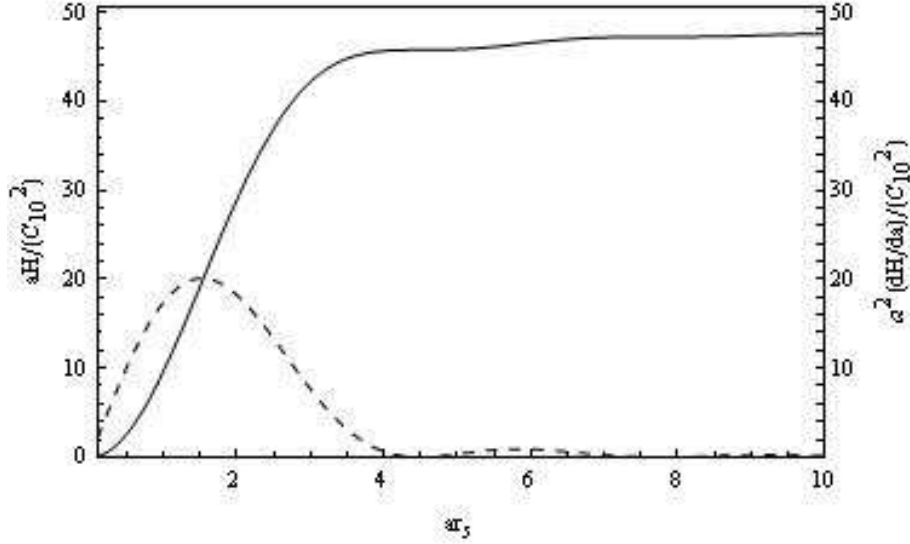


**Figure 3.** Helicity [solid curve, in units of  $(C_{10})^2/a$ ] and its derivative with respect to  $a$  [dashed curve, in units of  $(C_{10})^2/a^2$ ] versus  $ar_s$ , for the composite equipartitioned state with  $n = 1, 2, 3$  and  $0 \leq m \leq n$ .

## 4.2 Relaxation into equipartition

We now test the hypothesis that the force-free magnetic field evolves to energy equipartition. That is, we suppose that the relative weightings ( $C_{nm}$ ) of the modes adjust until each mode contributes equally to the total energy,  $W_T = N(N+1)W_{10}$  (for  $1 \leq n \leq N$ ,  $0 \leq m \leq n$ ). In ideal MHD, this cannot happen resistively. We postulate instead that it happens in the simulations because the random initial perturbations  $\delta\mathbf{B}$  (and concomitant fluid velocity perturbations  $\delta\mathbf{v}$ ) conspire to produce a nonzero mean electromotive field  $\langle \delta\mathbf{v} \times \delta\mathbf{B} \rangle \neq 0$  as they “unwind”, just like the  $\alpha$  effect in mean-field MHD (Biskamp 1993).

A force-free magnetic field relaxing via the  $\alpha$  effect seeks out a state which minimizes its helicity at a nonzero value, as observed in spheromaks (Taylor 1986). We find  $\partial H/\partial a = 0$  at  $ar_s = 4.49$  (where  $r_s$  is the radius of the model neutron star), the same conclusion reached by Taylor (1986) (see Fig. 3). This result applies to any combination of modes in equipartition, because  $W_T$  is proportional to  $W_{10}$ , and the energy of the  $(1,0)$  mode is minimized at  $ar_s = 4.49$ . Hence, Taylor’s minimum eigenvalue for axisymmetric spheromak eigenfunctions applies just as well to nonaxisymmetric eigenfunctions if the modes tend towards equipartition. We plot the helicity and its derivative for the composite equipartitioned state as functions of  $a$  in Fig. 3; the local minimum at  $a = 4.49r_s^{-1}$  is apparent. The helicity is calculated over the stellar volume, not out to infinity. This choice is bound up in the physics of the boundary conditions, which is discussed further at the end of this section and in Section 6.

The total helicity  $H_T$  is related to the total energy by  $H_T = 2\mu_0 W_T/a$ . Therefore, if the field is to change from a random configuration (where all  $C_{nm}$  are equal) to an equipartitioned one (where all modes contribute equal energy) while keeping both helicity and energy constant,  $a$  must remain constant as well. We designate this final state as State A. If, on the other hand, the field is allowed to convert its energy into, say, kinetic energy (e.g., random fluid motions in the MHD simulation),  $a$  can change to minimize  $W_T$  independently. We designate the corresponding final state as State B. We present the values of the mode coefficients  $C_{nm}$  achieved through these two scenarios in Table 1. Note that, for all four states, all constants  $C_{nm}$  increase from their initial values except for the  $(3,2)$  and  $(3,3)$  modes. Although  $C_{nm}$  takes higher values in State B than in State A, State B actually has a lower magnetic energy, due to the decrease in  $a$ .

We plot magnetic field lines of the initial state, State A, and State B in Figs. 4a, 4b, and 4c respectively. The two final states are similar in shape, with State B having a larger radius  $r_M$ , defined as (Braithwaite & Nordlund 2006)

$$r_M = \left( \frac{\int dV B^2 r^2}{\int dV B^2} \right)^{1/2}. \quad (10)$$

As the star does not have an actual surface, we use  $r_M$  as a proxy for the characteristic spatial extent of the field. Specifically, we find  $r_M/r_s = 0.71$ ,  $0.85$ , and  $1.0$  for the initial state, State A, and State B respectively. Fig. 4 is to be compared with the bottom left panel of Fig. 6 in Braithwaite and Nordlund (2006), which depicts the state achieved by the ideal-MHD simulation

**Table 1.** Parameters and constants of the initial and final states of the force-free magnetic field, under four evolutionary scenarios without diffusion. The force-free parameter  $a$  is measured in units of  $r_s^{-1}$ . The constants  $C_{nm}$  are measured in units of  $C_{10}$  at the start of the pre-diffusion phase, denoted by  $C$ .

Scenario	$ar_s$	$C_{10}/C$	$C_{11}/C$	$C_{20}/C$	$C_{21}/C$	$C_{22}/C$	$C_{30}/C$	$C_{31}/C$	$C_{32}/C$	$C_{33}/C$
Initial state	7.0	1.0	1.0	1.0	1.0	1.0	1.0	1.0	1.0	1.0
State A: equipartition, $H_T$ , $W_T$ , and $a$ constant	7.0	11	11	8.1	4.7	2.3	7.0	7.0	0.90	0.37
State B: equipartition, $H_T$ constant	4.5	11	11	8.4	4.8	2.4	8.8	8.8	1.1	0.47
State C: mean-field MHD, $H_T$ , $W_T$ , and $a$ constant	7.0	20	14	8.0	4.1	1.6	5.6	5.3	0.60	0.21
State D: mean-field MHD $H_T$ constant	4.5	21	15	8.1	4.2	1.7	5.7	5.4	0.61	0.21

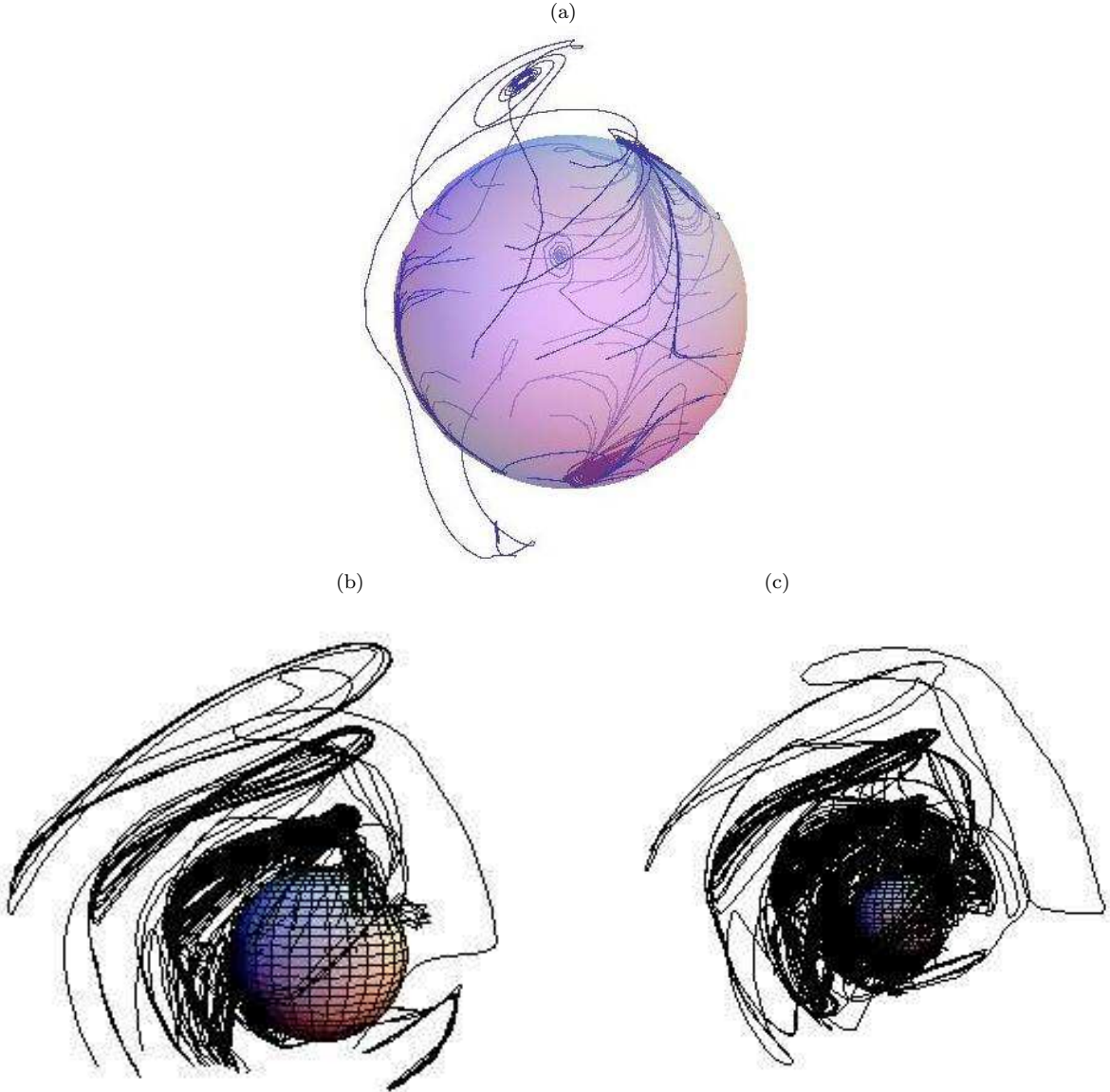


**Figure 4.** Magnetic field configurations produced by the evolutionary hypotheses in Section 4.2. (a) Initial random field, with  $C_{nm} = 1$  for all  $1 \leq n \leq 3$ ,  $0 \leq m \leq n$ , and  $ar_s = 7.0$ . (b) Final force-free field in State A, with  $C_{10} = 11$ ,  $C_{11} = 11$ ,  $C_{20} = 8.1$ ,  $C_{21} = 4.7$ ,  $C_{22} = 2.3$ ,  $C_{30} = 7.0$ ,  $C_{31} = 7.0$ ,  $C_{32} = 0.90$ ,  $C_{33} = 0.37$ , and  $ar_s = 7.0$ . (c) Final force-free field in State B, with  $C_{10} = 11$ ,  $C_{11} = 11$ ,  $C_{20} = 8.4$ ,  $C_{21} = 4.8$ ,  $C_{22} = 2.4$ ,  $C_{30} = 8.8$ ,  $C_{31} = 8.8$ ,  $C_{32} = 1.1$ ,  $C_{33} = 0.47$ , and  $ar_s = 4.5$ . The shaded sphere is at a radius  $r_s$ .





**Figure 5.** Magnetic field configurations produced by the evolutionary hypotheses in Section 4.3. (a) Final force-free field in State C, with  $C_{10} = 20$ ,  $C_{11} = 14$ ,  $C_{20} = 8.0$ ,  $C_{21} = 4.1$ ,  $C_{22} = 1.6$ ,  $C_{30} = 5.6$ ,  $C_{31} = 5.3$ ,  $C_{32} = 0.60$ ,  $C_{33} = 0.21$ , and  $ar_s = 7$ . (b) Final force-free field in State D, with  $C_{10} = 21$ ,  $C_{11} = 15$ ,  $C_{20} = 8.1$ ,  $C_{21} = 4.2$ ,  $C_{22} = 1.7$ ,  $C_{30} = 5.7$ ,  $C_{31} = 5.4$ ,  $C_{32} = 0.61$ ,  $C_{33} = 0.21$ , and  $ar_s = 4.5$ . The shaded sphere is at a radius  $r_s$ .

after 9 Alfvén crossing times of nondiffusive evolution. Qualitatively, the results are similar. Note how field lines form toroidal loops around the star in both the numerical and analytical calculations. The toroidal loops are wound closer to the star in Fig. 4c than in Fig. 4b, indicating that State B resembles Braithwaite and Nordlund (2006) more closely than State A. Also note that the “surface” of the star is located at  $r = r_s$  (where we also initialise the field lines), unlike in Fig. 6 of Braithwaite and Nordlund (2006), where the sphere is at  $r = 0.3r_s$ . Our model star does not have a hard boundary, and we do not match the “interior” force-free field to an “exterior” potential field at  $r = r_s$ .

Imposing a boundary condition at  $r = r_s$ , such as a conducting wall (more appropriate for laboratory plasmas) (Salingaros 1990), balance between external plasma pressure and internal magnetic pressure (Zhugzhda 1996; Vandas, Romashets, & Watari 2003), and force balance with an external magnetic field (Low & Berger 2003), affects the relaxation path and final state (Taylor 1986; Botha & Evangelidis 2004). The problem of matching a force-free field to an external field is nontrivial (Broderick & Narayan 2007), requiring  $a$  to vary (dis)continuously along the interface (plus the existence of non-force-free regions in the star). This matter is discussed in more detail in Section 6. Another potential issue is that, while the conductivity certainly damps the higher modes more quickly in a realistic field, as in the simulations, this is not true for the special case of force-free fields, where  $\nabla^2 \mathbf{B} = -a^2 \mathbf{B}$  for all  $(l, m)$ . This is another argument against the realism of force-free fields.

### 4.3 Blackman and Field (2004) mean-field dynamo

In the previous section, we do not advance a theory for how the parameter  $a$  and the constants  $C_{nm}$  change with time. We simply postulate an end state which fulfills energy equipartition and which is linked to the initial state by globally conserved quantities. In this section, we model the evolution more closely by applying a model developed by Blackman and Field (2004). This model is intended by the authors to be applicable to both astrophysical phenomena (such as stellar coronae) and laboratory plasma experiments. Blackman & Field (2004) explicitly sidestepped discussion of physical boundary conditions (particularly current closure) by utilizing periodic boundary conditions instead.

The model, rooted in the principles of mean-field MHD, gives a recipe for the coupled evolution of the spatially-averaged helicity on two length scales (one large, one small), as well as the spatially-averaged fluid vorticity and electromotive field. Upon splitting the magnetic field, vector potential, and current density into (slowly varying) large-scale and (turbulent) small-scale components, the volume-averaged induction equation and Faraday’s law imply

$$\partial_t H_1 = 2\langle \bar{\epsilon} \cdot \bar{\mathbf{B}} \rangle - 2\eta \langle \bar{\mathbf{B}} \cdot \bar{\mathbf{J}} \rangle \quad (11)$$

and

$$\partial_t H_2 = 2\langle \bar{\epsilon} \cdot \bar{\mathbf{B}} \rangle - 2\eta \langle \mathbf{b} \cdot \mathbf{j} \rangle. \quad (12)$$

**Table 2.** Poloidal flux, toroidal flux, and ratio of poloidal flux to toroidal flux, for the random initial state and States A–D. The fluxes are expressed in units of  $Cr_s^{-2}$ , where  $C$  is the initial value of the coefficient  $C_{10}$ .

State	Poloidal flux	Toroidal flux	Poloidal flux/toroidal flux
Random state	1.3	2.6	0.50
State A	14	20	0.70
State B	34	31	1.1
State C	27	22	1.2
State D	22	47	0.47

In (12)–(13),  $\eta$  is the magnetic diffusivity,  $H_1$  and  $H_2$  are the large- and small-scale magnetic helicities respectively,  $\overline{\mathbf{B}}$  and  $\mathbf{b}$  are the large- and small-scale magnetic fields,  $\overline{\mathbf{J}}$  and  $\mathbf{j}$  are the large- and small-scale current densities, and  $\overline{\boldsymbol{\varepsilon}} = -\overline{\mathbf{E}} + \eta(\overline{\mathbf{B}} \cdot \overline{\mathbf{J}})$  is the turbulent electromotive field. By utilising Ampère’s Law, Faraday’s Law, and the incompressible Navier-Stokes equation, Blackman and Field (2004) derived the following closed set of evolution equations for the spatially averaged helicities ( $H_1$  and  $H_2$ ), vorticity  $H_V = \langle \mathbf{v} \cdot \nabla \times \mathbf{v} \rangle$ , electromotive field  $Q$ , and energy  $\epsilon$ :

$$\frac{\partial h_1}{\partial \tau} = -2Qh_1^{1/2}(k_1/k_2)^{1/2} - 2h_1(k_1/k_2)^2/R_M, \quad (13)$$

$$\frac{\partial h_2}{\partial \tau} = 2Qh_1^{1/2}(k_1/k_2)^{1/2} - 2h_2/R_M, \quad (14)$$

$$\frac{\partial h_v}{\partial \tau} = -2(1 - k_1/k_2)(k_1/k_2)^{1/2}Qh_1^{1/2} - 2h_v/R_V, \quad (15)$$

$$\frac{\partial Q}{\partial \tau} = -(k_1/k_2)^{1/2}h_1^{1/2}(1/3)(h_2 - h_v) + (k_1/k_2)^{3/2}h_1^{1/2}\epsilon/3 - \epsilon^{1/2}fQ, \quad (16)$$

$$\frac{\partial \epsilon}{\partial \tau} = -2(1 - k_1/k_2)(k_1/k_2)^{1/2}Qh_1^{1/2} - 2\epsilon/R_V. \quad (17)$$

In (14)–(18), we define  $k_1$  and  $k_2$  as the characteristic large- and small-scale wavenumbers,  $R_V = H_2(0)^{1/2}/\nu k_2^{1/2}$  (where  $\nu$  is viscosity),  $R_M = H_2(0)^{1/2}/\eta k_2^{1/2}$ ,  $h_v = H_V/k_2^2 H_2(0)$ ,  $h_1$  and  $h_2$  are the large- and small-scale helicities normalised to  $H_2(0)$ ,  $Q = -\overline{\boldsymbol{\varepsilon}}_{\parallel}/k_2 H_2(0)$  is the component of the turbulent electromotive field parallel to  $\overline{\mathbf{B}}$ ,  $\epsilon = \langle \mathbf{v}^2 \rangle/k_2 H_2(0)$ , where  $\mathbf{v}$  is the turbulent fluid velocity,  $\tau = tk_2^{3/2} H_2(0)^{1/2}$ , and  $f \sim 1$  is a dimensionless constant which parametrizes the (unspecified) microphysical dissipation (Blackman & Field 2004). The notation ‘(0)’ denotes an initial value.

Let us now look at what happens in the steady state. From (14) and (15), the steady-state helicities satisfy

$$h_2 = (k_1/k_2)^2 h_1. \quad (18)$$

For our force-free modes (3)–(5), we can write  $k_{mn} \propto (n^2 + m^2)^{1/2}$ . Suppose that the two-mode result (19) can be generalized to apply to all the modes in a linear combination. We designate the final relaxed state with  $C_{nm}$  related through (19) as State C if both helicity and magnetic energy are kept constant throughout relaxation, and as State D if only the helicity is kept constant. Magnetic field lines for States C and D are shown in Figs. 5a and 5b respectively. These states *do not* obey the equipartition relation. Note that States C and D are very similar (see also Table 1), while A and B are less so, indicating a weaker dependence of  $H_T$  on  $a$ . The values of  $r_M/r_s$  are 0.77 and 0.78 for States C and D respectively. As evident from Table 1, all  $C_{nm}$  in States C and D are smaller than in States A and B, except for  $C_{1m}$ . In fact, the axisymmetric (1,0) mode dominates in States C and D, being approximately 20 times greater than in the initial state, giving these states a more toroidal shape (see Figs. 5a and 5b).

To quantify further the ‘shape’ of the field, we compute the poloidal flux  $\Phi_\theta$  and toroidal flux  $\Phi_\phi$  from

$$\Phi_\theta = \int_0^{2\pi} d\phi \int_0^{r_s} dr \, r B_\theta(r, \pi/2, \phi) \quad (19)$$

$$\Phi_\phi = \frac{1}{2} \int_0^\pi d\theta \int_0^{r_s} dr \, r B_\phi(r, \theta, 0) + \frac{1}{2} \int_0^\pi d\theta \int_0^{r_s} dr \, r B_\phi(r, \theta, \pi). \quad (20)$$

The results are listed in Table 2. In all four final states,  $\Phi_\theta$  and  $\Phi_\phi$  are comparable. This is a natural property of the linked toroidal-poloidal field structure necessary for long-term MHD stability. Again, we see that nonaxisymmetric force-free modes play a key role, this time in ensuring long-term stability.

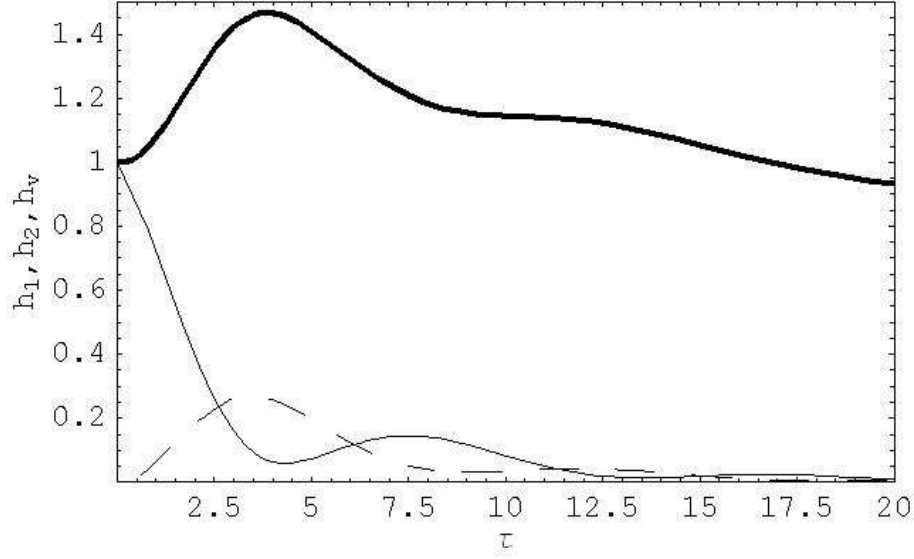


**Figure 6.** Dimensionless helicities of the (1,1) mode ( $h_1$ , thick solid curve), (3,3) mode ( $h_2$ , thin solid curve), and vorticity ( $h_v$ , dashed curve) as functions of  $\tau$ .  $h_1$  and  $h_2$  are initially equal (the modes are in equipartition) and  $h_v$  is initially zero. The dimensionless physical parameters  $f$ ,  $R_M$ , and  $R_V$  are taken to be 1, 10, and 10 respectively.

## 5 DIFFUSIVE EVOLUTION

In the second stage of the numerical experiments described by Braithwaite and Nordlund (2006), the resistivity is switched on and the magnetic field obtained at the end of the (ideal-MHD) first stage is allowed to relax by Ohmic diffusion (Braithwaite & Spruit 2006). What are the implications for our analytic model?

If the field remains in a linear superposition of quasistatic force-free modes, the linear independence of the modes ensures that they all decay at the same rate, proportional to the electrical conductivity  $\sigma$ :

$$dC_{nm}/dt = (a^2/\mu_0\sigma)C_{nm}. \quad (21)$$

If the force-free parameter  $a$  also remains constant throughout the diffusion process, it is evident that the structure of field lines, e.g. the quantity  $r_M$  and poloidal-to-toroidal flux ratio, also remain unchanged. This is contrary to the results of Braithwaite and Nordlund, who found that the field becomes more poloidal and dipole-like as it diffuses outwards (Braithwaite & Nordlund 2006). By implication, the field does not remain force free (with constant  $a$ ) in the resistive stage of the simulations. We note that an extra term is added to the magnetic field diffusion equation if  $a$  is nonuniform, since the term  $\eta\nabla^2\mathbf{B}$  now becomes  $-a^2\eta\mathbf{B} - \eta(\nabla a) \times \mathbf{B}$ , which affects the shape of the field as it diffuses, depending on  $\nabla a$ .

However, if we allow the energy to vary freely and even allow some loss of helicity (Braithwaite & Spruit 2006), some of the magnetic energy at the start of the resistive stage is converted into fluid kinetic energy  $\epsilon$ , inducing a turbulent dynamo which regenerates the field (or, at least, exchanges helicity between small and large scales). Following Blackman and Field (2004), we consider two force-free modes with sufficiently different characteristic wavenumber  $k$  [modes (1,1) and (3,1), for example] and let them evolve from equipartition as per (14)–(18). The results are plotted in Fig. 6 and reveal some general trends. First of all, we find that the turbulent vorticity  $h_v$ , which starts at zero, increases briefly then dies away, controlled by  $R_V$  ( $h_v$  falls away slower for larger  $R_V$ , i.e. smaller viscosity). Secondly, the long-wavelength mode increases at first but then decreases while the short-wavelength mode decreases immediately (and faster). The rates at which the modes decay are controlled by the quantity  $R_M$ ; the larger the magnetic diffusivity, the faster the decay. Thus, in the long term, the lower  $n$  and  $m$  modes dominate, until all the higher order and nonaxisymmetric modes vanish; a force-free field which is a linear combination of several modes can decay into an axisymmetric Taylor state, given enough time and a mediating turbulent vorticity. We stress again, however, that this dynamo picture is one of many possibilities, and it does not take into account superfluid and stratification effects in a neutron star.

## 6 DISCUSSION

We show in this paper that an initial magnetic field which is a linear combination of equally weighted, force-free modes can relax without diffusion, preserving magnetic helicity, to an equipartitioned state which possesses a linked poloidal-toroidal geometry (with toroidal flux dominating), just like the end result of the first (nondiffusive) stage of the numerical simulations by

Braithwaite and collaborators (Braithwaite & Nordlund 2006; Braithwaite & Spruit 2006). Alternatively, a turbulent, mean-field MHD dynamo model (Blackman & Field 2004) can be used to prescribe the evolution of the force-free field, allowing helicity to be exchanged between small and large scales through the agency of a turbulent electromotive field (and growth of small-scale hydrodynamic vorticity). Applying this particular model to our initial state, we again obtain a final configuration which qualitatively resembles the numerical results of Braithwaite and Nordlund (2006), but with smaller root-mean-square size  $r_M$ . *The inclusion of nonaxisymmetric force-free modes is important to obtain good agreement.*

A force-free field decays uniformly when a uniform resistivity is switched on, keeping the relative weighting of its modes (and hence its three-dimensional structure) constant. This behaviour is not observed in the numerical simulations, where instead the field diffuses outwards over time into a dipolar shape (Braithwaite & Nordlund 2006; Braithwaite & Spruit 2006). If, however, a turbulent electromotive force is allowed to operate, we show that the higher-order modes decay faster, and the magnetic field tends overall towards the Taylor axisymmetric state (which is dominated by toroidal flux at  $ar_s = 4.49$ ).

We conclude by speaking briefly about the vital issue of boundary conditions at the stellar surface. In this paper, we assume (for the sake of analytic simplicity) that the magnetic field is force-free everywhere, because our main goal is to elucidate the central role played by the nonaxisymmetric modes. In order to preserve finite helicity and energy, we are forced to integrate (artificially)  $\mathbf{A} \cdot \mathbf{B}$  and  $B^2/2\mu_0$  over just the volume of the star, rather than over all space. Hence the helicity and energy we compute are semiquantitative approximations. It is natural to try and correct this shortcoming by matching a force-free field in the stellar interior to a current-free (potential) field in an insulating atmosphere above the stellar surface (Broderick & Narayan 2007). The matching conditions are popularly taken as: (i) normal component of  $\mathbf{B}$  is continuous at the surface (which uniquely determines the external field) and (ii) the jump in the tangential component of  $\mathbf{B}$  is proportional to the surface (skin) current (and indeed uniquely determines the latter). However, this prescription hides a subtle flaw: current continuity ( $\nabla \cdot \mathbf{J} = 0$ ) is violated at the surface, because it is impossible, in general, for the skin current leaving (entering) a surface patch sideways to balance the volume current  $\mu_0^{-1}aB_r$  entering (leaving) the patch from below. The root of this apparent paradox concerning current closure can be traced back to the following classic theorem of magnetostatics: a magnetic field which is force free everywhere within a finite volume cannot match to an external field which is potential everywhere (Priest 1984)<sup>2</sup>. [Physically, solutions with surface currents are not appealing, because conductivities drop off towards the surface of the star (Braithwaite 2008). In this way, Broderick and Narayan’s (2007) treatment is problematic; surface currents are an artifact arising out of the matching problem and are accompanied by an artificial surface  $\mathbf{J} \times \mathbf{B}$  force.]. One way to resolve the paradox is to allow currents to flow in the atmosphere above the surface, e.g. through discrete structures like magnetic arcades (cf. the Sun). Under these circumstances, the force-free parameter  $a(\mathbf{x})$  must vary with position, and the matching conditions at any interface reduce to continuity of (i) the normal component of  $\mathbf{B}(\mathbf{x})$ , and (ii)  $a(\mathbf{x})$  (over one polarity of  $\mathbf{B}$ ), which are solved iteratively (Wheatland 2006). Loss of helicity through parts of the surface can occur (Braithwaite & Spruit 2006), although care must be taken to use appropriate boundary conditions on the slow relaxation time-scale. Another way to resolve the paradox is to create a non-force-free (i.e., stressed) region within the star, through which the currents can close. Imposing boundary conditions at the stellar surface which satisfy  $\nabla \cdot \mathbf{J} = 0$  in this scenario is a nontrivial task.

Both resolutions of the matching paradox outlined above may carry important implications for magnetar astrophysics. The first suggests the likelihood of magnetic activity (e.g. reconnection between magnetic arcades) in the magnetosphere, accompanied perhaps by radio and X-ray bursts. The second suggests that magnetic stresses may cause crust cracking in non-force-free regions. Note that neutron star magnetosphere models have popularly included surface currents in the past [e.g., Goldreich and Julian (1969), Ruderman (1975), Mestel *et al.* (1985), and Arons (1993)]. This paper exposes some of the limitations of analytic methods. A better way to study such possibilities *self-consistently* is to extend the simulations in Braithwaite and Nordlund (2006) and elsewhere to treat in more detail the mechanical behaviour of the stellar interior.

## ACKNOWLEDGMENTS

We thank Paul Cally for alerting us to the impossibility of matching an internal force-free field to an external potential field. We also thank the reviewer for his/her invaluable input and constructive criticism, which have improved this paper greatly. This work is supported by the Melbourne University International Postgraduate Research Scholarship.

<sup>2</sup> The theorem follows from the identity

$$\int dV \mathbf{x} \cdot (\mathbf{J} \times \mathbf{B}) = \frac{1}{2\mu_0} \int dV |\mathbf{B}|^2 + \frac{1}{2\mu_0} \int dS \cdot [2(\mathbf{x} \cdot \mathbf{B})\mathbf{B} - |\mathbf{B}|^2\mathbf{x}], \quad (22)$$

if we consider a spherical surface of radius  $R$  that fully encloses the force-free region and let  $R \rightarrow \infty$ .

## REFERENCES

- Arons J., 1993, *ApJ*, 408, 160
- Barnes C.W., Fernandez J.C., Henins I., Hoida H.W., Jarboe T.R., Knox S.O., Marklin G.J., McKenna K.F., 1986, *Phys. Fluids*, 29, 3415
- Biskamp D., 1993, *Nonlinear magnetohydrodynamics*, Cambridge Monographs on Plasma Physics 1. Cambridge University Press, Cambridge
- Blackman E.G., Field G.B., 2004, *Phys. of Plasmas*, 11, 3264
- Botha G.J.J., Evangelidis E.A., 2004, *MNRAS*, 350, 375
- Braithwaite J., private communication
- Braithwaite J., Nordlund A., 2006, *A&A*, 450, 1077
- Braithwaite J., Spruit H.C., 2004, *Nature*, 431, 819
- Braithwaite J., Spruit H.C., 2006, *A&A*, 450, 1097
- Brandenburg A., Subramanian K., 2005, *Phys. Rep.*, 416, 1
- Broderick A.E., Narayan R., 2007, *MNRAS*, 383, 943
- Chandrasekhar S., 1956, *Proc. Nat. Acad. Sci.*, 42, 1
- Chandrasekhar S., Kendall P.C., 1957, *ApJ*, 126, 457
- Charbonneau P., MacGregor K.B., 1996, *ApJ*, 473, L59
- Duncan R.C., Thompson C., 1992, *ApJ*, 392, L9
- Donati J.-F., Howarth I.D., Bouret J.-C., Petit P., Catala C., Landstreet J., 2006, *MNRAS*, 365, L6
- Donati J.-F. et al., 2006, *MNRAS*, 370, 629
- Ferrario L., Wickramasinghe D., 2006, *MNRAS*, 367, 1323
- Gaensler B.M., Gotthelf E.V., Vasisht G., 1999, *ApJ*, 526, L37
- Gaensler B.M., McClure-Griffiths N.M., Oey M.S., Haverkorn M., Dickey J.M., Green A.J., 2005, *ApJ*, 620, L95
- Goldenbaum G.C., Irby J.H., Chong Y.P., Hart G.W., 1980, *Phys. Rev. Lett.*, 44, 390
- Goldreich P., Julian W.H., 1969, *ApJ*, 157, 869
- Goldreich P., Reisenegger A., 1992, *ApJ*, 395, 250
- Goossens M., Tayler R.J., 1980, *MNRAS*, 193, 833
- Heger A., Woosley S.E., Langer N., Spruit H.C., 2003, in Maeder A., Eenes P., eds, *Proc. IAU Symp. Vol. 215, Stellar Evolution*. Astron. Soc. Pac., San Francisco, p.591
- Hurley K. et al., 2005, *Nature*, 434, 1098
- Janos A., Hart G.W., Yamada M., 1985, *Phys. Rev. Lett.*, 55, 2868
- Jarboe T.R., Henins I., Hoida H.W., Linford R.K., Marshall J., Platts D.A., Sherwood A.R., 1980, *Phys. Rev. Lett.*, 45, 1264
- Jordan D.W., Smith P., 1999, *Nonlinear ordinary differential equations: an introduction to dynamical systems*. Oxford University Press, Oxford.
- Kaspi V.M., McLaughlin M.A., 2005, *ApJ*, 618, L41
- Knox S.O., Barnes C.W., Marklin G.J., Jarboe T.R., Henins I., Hoida H.W., Wright B.L., 1986, *Phys. Rev. Lett.*, 56, 842
- Kouveliotou C. et al., 1994, *Nature*, 368, 125
- Kouveliotou C. et al., 1998, *Nature*, 393, 235
- Low B.C., Berger M.A., 2003, *ApJ*, 589, 644
- McLaughlin M.A. et al., 2003, *ApJ*, 591, L135
- Melatos A., 1999, *ApJ*, 519, L77
- Mereghetti S., 2000, in Kouveliotou C., Ventura J., van den Heuvel E., eds., *The Neutron Star – Black Hole Connection*. Kluwer Academic, London, p. 351
- Mestel L., Robertson J.A., Wang Y.-M., Westfold K.C., 1985, *MNRAS*, 217, 443
- Moss D., 2001, in Mathys G., Solanki S.K., Wickramasinghe D.T., eds., *Magnetic Fields across the Hertzsprung-Russell Diagram*, ASP Conference Series, Vol. 248. Astronomical Society of the Pacific, San Francisco, p. 305
- Moss D., 2003, *A&A*, 403, 693
- Palmer D.M. et al., 2005, *Nature*, 434, 1107
- Petit V., Wade G.A., Drissen L., Montmerle T., 2007, preprint (astro-ph/0709.4526v1)
- Prendergast K.H., 1956, *ApJ*, 123, 498
- Popov S.B., Prokhorov M.E., 2006, *MNRAS*, 367, 732
- Priest E.R., 1984, *Solar magnetohydrodynamics*. D. Reidel Publishing Company, Dordrecht
- Rosenbluth M.N., Bussac M.N., 1979, *Nucl. Fusion*, 19, 489
- Rothschild R.E., Kulkarni S.R., Lingenfelter R.E., 1994, *Nature*, 368, 432
- Ruderman M., 1975, *Ann. N.Y. Acad. Sci.*, 257, 127

- Salingeros N.A., 1990, *Appl. Phys. Lett.*, 56, 617  
 Spruit H., 1992, *A&A*, 381, 923  
 Tayler R.J., 1980, *MNRAS*, 191, 151  
 Taylor J.B., 1986, *Rev. Mod. Phys.*, 58, 741  
 Thompson C., Duncan R.C., 1995, *MNRAS*, 275, 255  
 Thompson C., Duncan R.C., 1996, *ApJ*, 473, 322  
 Turner W.C., Goldenbaum G.C., Granneman E.H.A., Hammer J.H., Hartman C.W., Prono D.S., Taska J., 1983, *Phys. Fluids*, 26, 1965  
 van Assche W., Tayler R.J., Goossens M., 1982, *A&A*, 109, 166  
 Vandas M., Romashets E.P., Watari S., 2003, in *Proc. ISCS 2003 Symp.*, ESA SP-535, *Solar Variability as an Input to the Earth's Environment*. ESA Publications, Noordwijk, p. 583  
 Vink J., 2008, *Advances in Space Res.*, 41, 503  
 Vink J., Kuiper L., 2006, *MNRAS*, 370, L14  
 Wheatland M.S., 2006, *Sol. Phys.*, 238, 29  
 Woltjer L., 1964, *ApJ*, 140, 1309  
 Woods P.M., Thompson C., 2006, in Lewin W., van der Klis M., eds, *Compact stellar X-ray sources*, Cambridge Astrophysics Series, No. 39. Cambridge University Press, Cambridge, p. 547  
 Wright G.A.E., 1973, *MNRAS*, 162, 339  
 Yamada M. et al., 1981, *Phys. Rev. Lett.*, 46, 188  
 Zhugzhda Y.D., 1996, *Phys. of Plasmas*, 3, 10

This paper has been typeset from a  $\text{\TeX}$ / $\text{\LaTeX}$  file prepared by the author.